Modelling of Aging Response in Glassfibre-reinforced Concrete Flexural Specimens

CHOTE SORANAKOM
Graduate Research Assistant ,Department of Civil and Environmental Engineering, Arizona State University, Tempe, AZ, 85287, email: mrchote@yahoo.com

MASOUD YEKANI-FARD
Graduate Research Assistant, Department of Civil and Environmental Engineering, Arizona State University, Tempe, AZ, 85287, email: Masoud.Yekanifard@asu.edu

BARZIN MOBASHER
PhD, PE, Professor, Department of Civil and Environmental Engineering, Arizona State University, Tempe, AZ, 85287, email: barzin@asu.edu

Abstract

A constitutive law for glassfibre-reinforced concrete (GFRC), consisting of a bilinear tension with residual strength and elastic-perfectly-plastic compression stress strain model, is proposed. The applicability of the model for characterisation and prediction of long-term flexural behaviour of GFRC materials is studied. Flexural test data of control and mixtures containing metakaolin subjected to hot-water-accelerated aging at three levels (unaged, 28 and 84 days of aging) were back-calculated to obtain material parameters and establish their relationships with aging. At typical high fibre dosages of 5% by weight, the flexural response shows deflection hardening behaviour followed by brittle failure. The material behaviour is described by four parameters: Young's modulus, post-cracking modulus, first cracking strain and strain at peak stress. Once the relationships between the parameters and age were established, the time-dependent flexural performance of the control and metakaolin mixes were simulated. Results reveal that use of metakaolin reduces the deterioration of moment and ductility as material ages with time.

1. Introduction

Glassfibre-reinforced concrete (GFRC) is a cement-based composite that has gained popularity in the manufacturing of cladding panels. The long-term properties of the composite exposed to humid environments exhibit embrittlement and loss of flexural strength over time[1, 2]. Deterioration is caused primarily by the chemical and physical processes. Glassfibres chemically degrade in the alkaline hydrated cement environment and lose some of their tensile strength. The physical cause of strength reduction comes from the hydration products, especially calcium hydroxide which fills the spaces between the fibre filaments and reduces the compliance of the fibre yarn. This causes stress concentration and excessive bonding at the surface of fibres, changing the fibre pull-out mechanism to fibre breakage under tension loading. The aging problem of glassfibre in an alkaline environment led to the development of several measures such as the invention of alkali-resistant glassfibres, use of polymer emulsions in the cement matrix, and the addition of pozzolanic materials to react with calcium hydroxide. In order to evaluate the improvement of GFRC for various treatments, accelerated aging procedures have been developed and test results can be correlated with naturally aged specimens collected in the field[3, 4].

An analytical model has recently been developed for predicting the flexural behaviour of fibre-reinforced concrete[5, 6]. This approach has been extended to both strain softening and strain hardening materials[7]. Therefore a rational modelling approach for GFRC is possible. The main objective of this paper is to develop a procedure for using the aging flexural test data to predict the long-term flexural behaviour of GFRC.

2. Constitutive law for homogenized fibre-reinforced concrete

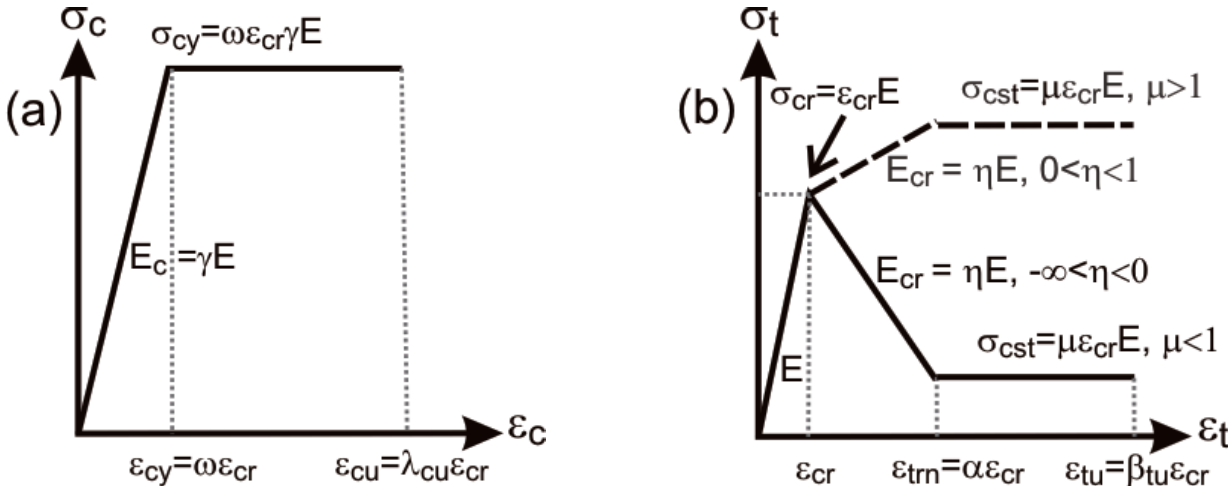

Figure 1: Material models for homogenized fibre-reinforced concrete: (a) compression model; and (b) tension model

A constitutive law for homogenized fibre-reinforced concrete is presented in Fig. 1. The compression response is described by an elastic-perfectly-plastic model. The compressive stress reaches its plastic limit σ_{cy} at yield point (ε_{cy}, σ_{cy}) and remains constant until the strain reaches the ultimate compressive strain ε_{cu}. The tension response is described by a trilinear model with an elastic range defined by E, and terminated at the first cracking tensile strain ε_{cr}. Then the response continues in the post-cracking region described by the post-cracking modulus E_{cr}; by setting E_{cr} to either a negative or a positive value, the same model can be used to simulate strain-softening or strain-hardening materials. The third region in the late tensile response is a constant stress range defined as σ_{cst}, which can be set to any value, starting at the transition strain ε_{trn}. Finally the response is terminated at the ultimate tensile strain ε_{tu}. In order to derive the closed-form solutions for moment–curvature response in non-dimensional forms, the material parameters shown in Fig. 1(a) and (b) are defined as a combination of seven normalized parameters with respect to the intrinsic parameters E and ε_{cr} as shown in equations (1)–(3):

$$\omega = \frac{\varepsilon_{cy}}{\varepsilon_{cr}}; \quad \alpha = \frac{\varepsilon_{trn}}{\varepsilon_{cr}}; \quad \beta_{tu} = \frac{\varepsilon_{tu}}{\varepsilon_{cr}}; \quad \lambda_{cu} = \frac{\varepsilon_{cu}}{\varepsilon_{cr}} \tag{1}$$

$$\gamma = \frac{E_c}{E}; \quad \eta = \frac{E_{cr}}{E} \tag{2}$$

$$\mu = \frac{\sigma_{cst}}{E\varepsilon_{cr}} \tag{3}$$

In addition to material parameters for the model, the tensile strain at the bottom fibre ε_{tbot} and compressive strain at the top fibre ε_{ctop} are also defined in normalized forms as:

$$\beta = \frac{\varepsilon_{tbot}}{\varepsilon_{cr}}; \quad \lambda = \frac{\varepsilon_{ctop}}{\varepsilon_{cr}} \tag{4}$$

Both strains are linearly related through the normalized neutral axis parameter, *k* by:

$$\frac{\lambda\varepsilon_{cr}}{kd}=\frac{\beta\varepsilon_{cr}}{d-kd} \quad \text{or} \quad \lambda=\frac{k}{1-k}\beta \tag{5}$$

3. Closed-form solutions for moment–curvature response

Figure 2 shows three stages of stress–strain diagrams ($0<\beta\le 1$, $1<\beta\le\alpha$ and $\alpha<\beta\le\beta_{tu}$) as a function of the normalized bottom tensile strain β. These diagrams were used in the derivation of a closed-form solution for the moment–curvature diagram[5]. In the elastic stage 1, the stress diagram is unique, as shown in Fig. 2(a), while stages 2 and 3 have two possible scenarios: the compressive strain at the top fibre is either elastic ($0<\lambda\le\omega$) or plastic ($\omega<\lambda\le\lambda_{cu}$) and the derivations for these two stages were treated separately. The neutral axis depth ratio *k* is found by solving for equilibrium of forces. The moment capacity is then calculated from internal forces and the neutral axis location; the corresponding curvature is obtained by dividing the top compressive strain by the neutral axis depth.

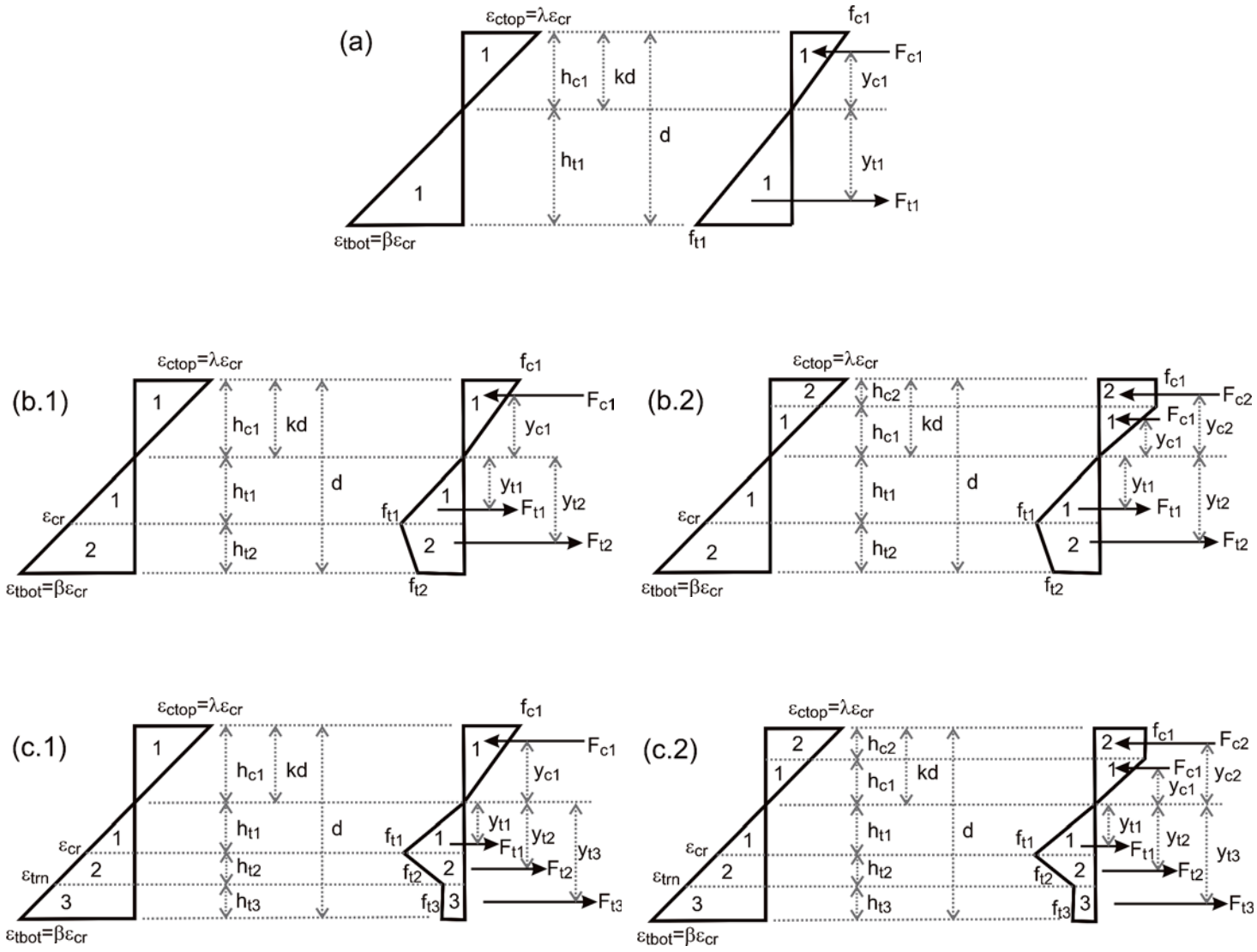

Figure 2: Stress–strain diagram at different stages of normalized tensile strain at the bottom fibre (β):
(a) $0<\beta\le 1$ and $0<\lambda\le\omega$;
(b.1) $1<\beta\le\alpha$ and $0<\lambda\le\omega$; (b.2) $1<\beta\le\alpha$ and $\omega<\lambda\le\lambda_{cu}$;
(c.1) $\alpha<\beta\le\beta_{tu}$ and $0<\lambda\le\omega$; (c.2) $\alpha<\beta\le\beta_{tu}$ and $\omega<\lambda\le\lambda_{cu}$

Finally, the moment M_i and curvature φ_i for each stage *i* are normalized with their cracking moment M_{cr} and cracking curvature φ_{cr} to obtain the normalized moment M_i' and curvature φ_i', respectively. Expressions for calculating the neutral axis/depth ratio, moment and curvature are given in equations (6) and (7) and Table 1:

$$M_i = M_i' M_{cr}; \quad M_{cr} = \frac{1}{6} b d^2 E \varepsilon_{cr} \tag{6}$$

$$\phi_i = \phi_i' \phi_{cr}; \quad \phi_{cr} = \frac{2\varepsilon_{cr}}{d} \tag{7}$$

Stage	k	M_i' and ϕ_i'
1 $0 < \beta \leq 1$	$k_1 = \begin{cases} \frac{1}{2} & \text{for } \gamma=1 \\ \frac{-1+\sqrt{\gamma}}{-1+\gamma} & \text{for } \gamma<1 \text{ or } \gamma>1 \end{cases}$	$M'_1 = \frac{2\beta\left[(\gamma-1)k_1^3 + 3k_1^2 - 3k_1 + 1\right]}{1-k_1}$ $\phi'_1 = \frac{\beta}{2(1-k_1)}$
2.1 $1<\beta\leq\alpha$ $0<\lambda\leq\omega$	$k_{21} = \frac{\beta^2\gamma + D_{21} - \sqrt{\gamma^2\beta^4 + D_{21}\gamma\beta^2}}{D_{21}}$ $D_{21} = \eta\left(\beta^2 - 2\beta + 1\right) + 2\beta - \beta^2\gamma - 1$	$M'_{21} = \frac{(2\beta\gamma + C_{21})k_{21}^3 - 3C_{21}k_{21}^2 + 3C_{21}k_{21} - C_{21}}{1-k_{21}}$ $C_{21} = \frac{-2\eta\beta^3 + 3\eta\beta^2 - 3\beta^2 - \eta + 1}{\beta^2}$ $\phi'_{21} = \frac{\beta}{2(1-k_{21})}$
2.2 $1<\beta\leq\alpha$ $\omega<\lambda\leq\lambda_{cu}$	$k_{22} = \frac{D_{22}}{D_{22} + 2\omega\gamma\beta}$ $D_{22} = \eta\left(\beta^2 - 2\beta + 1\right) + 2\beta + \omega^2\gamma - 1$	$M'_{22} = (3\omega\gamma + C_{22})k_{22}^2 - 2C_{22}k_{22} + C_{22}$ $C_{22} = \frac{2\eta\beta^3 - 3\eta\beta^2 + 3\beta^2 - \omega^3\gamma + \eta - 1}{\beta^2}$ $\phi'_{22} = \frac{\beta}{2(1-k_{22})}$
3.1 $\alpha<\beta\leq\beta_{tu}$ $0<\lambda\leq\omega$	$k_{31} = \frac{D_{31} - \sqrt{\gamma\beta^2 D_{31}}}{D_{31} - \beta^2\gamma}$ $D_{31} = \eta\left(\alpha^2 - 2\alpha + 1\right) + 2\mu(\beta - \alpha) + 2\alpha - 1$	$M'_{31} = \frac{(C_{31} - 2\beta\gamma)k_{31}^3 - 3C_{31}k_{31}^2 + 3C_{31}k_{31} - C_{31}}{k_{31} - 1}$ $C_{31} = \frac{3\left(\mu\beta^2 - \mu\alpha^2 - \eta\alpha^2 + \alpha^2\right) + 2\eta\alpha^3 + \eta - 1}{\beta^2}$ $\phi'_{31} = \frac{\beta}{2(1-k_{31})}$
3.2 $\alpha<\beta\leq\beta_{tu}$ $\omega<\lambda\leq\lambda_{cu}$	$k_{32} = \frac{D_{32}}{D_{32} + 2\omega\gamma\beta}$ $D_{32} = \omega^2\gamma + \eta\alpha^2 + 2(\mu\beta - \eta\alpha - \mu\alpha + \alpha) + \eta - 1$	$M'_{32} = (C_{32} + 3\omega\gamma)k_{32}^2 - 2C_{32}k_{32} + C_{32}$ $C_{32} = \frac{3\left(\mu\beta^2 - \mu\alpha^2 - \eta\alpha^2 + \alpha^2\right) + 2\eta\alpha^3 - \omega^3\gamma + \eta - 1}{\beta^2}$ $\phi'_{32} = \frac{\beta}{2(1-k_{32})}$

Table 1: Neutral axis depth ratio k, normalized moment M_i' and curvature φ_i' for each stage i of normalized tensile strain at bottom fibre (β)

As mentioned earlier, the compressive strain at the top fibre λ in stage 2 or 3 could be in either the elastic ($0< \lambda \leq \omega$) or plastic ($\omega < \lambda \leq \lambda_{cu}$) range, depending on the applied tensile strain β and neutral axis parameter k. The range can be identified by assuming $\lambda < \omega$ (Fig. 2(b.1) or 2(c.1)) and using the expression k_{21} or k_{31} in Table 1 to determine λ from equation (5). If $\lambda < \omega$ holds true, the assumption is correct, otherwise $\lambda > \omega$ and the expression k_{22} or k_{32} is used instead. Once, the neutral axis parameter k and the applicable case are determined, the appropriate expressions for moment and curvature in Table 1 and equations (6) and (7) are used.

3.1. Crack localisation rules and load–deflection prediction

Figure 3(a) shows a schematic drawing of four-point bending test with localisation of smeared crack that occurs in the mid-zone; while the zones outside the cracking region undergo unloading during softening[8, 9].

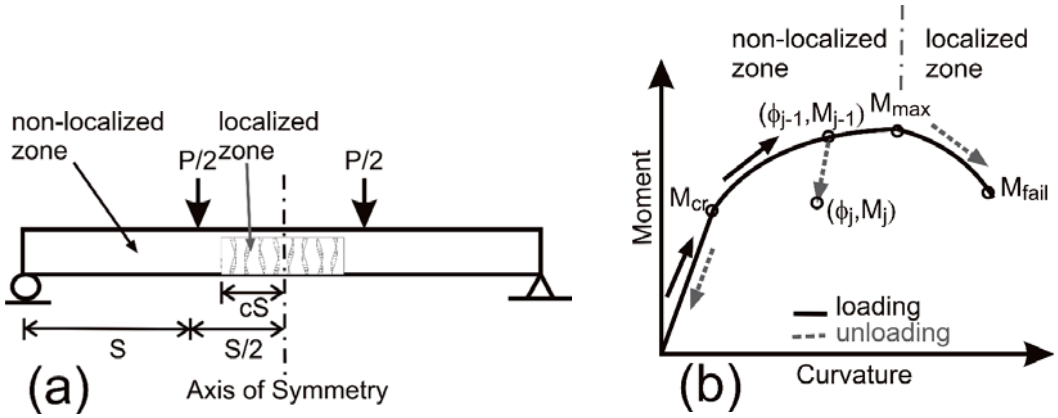

Figure 3: (a) Four -point bending test; (b) moment–curvature diagram and crack localization rules

The length of the localised zone is defined as '*cS*', representing the product of a normalized parameter *c* and loading-point spacing $S = L/3$, where L is the clear span. For the simulations of GFRC in this paper, it was assumed that cracks were uniformly distributed throughout the mid-zone and a value of $c = 0.5$ was used. As shown in Fig. 3(a), a typical moment–curvature diagram is divided into two portions: an ascending curve from 0 to M_{max} and a descending curve from M_{max} to M_{fail}. To predict load–deflection response, an array of load steps is derived from a series of discrete data points along the moment–curvature diagram. For each load step, the moment distribution along the length of a beam is obtained by static equilibrium and the corresponding curvature is obtained from a moment–curvature relationship and crack localization rule. When the specimen is loaded from 0 to M_{max}, the ascending portion of the diagram is used to identify the curvature. Beyond the maximum load, as the specimen undergoes softening, the curvature distribution depends on the localized or non-localized zones and its prior strain history (uncracked or cracked). For an uncracked section, the curvature unloads elastically. If the section has been loaded beyond cracking moment M_{cr}, the unloading curvature follows a quasi-linear recovery path expressed as:

$$\phi_j = \phi_{j-1} - \xi \frac{(M_{j-1} - M_j)}{EI} \qquad (8)$$

where φ_{j-1} and M_{j-1} represent the previous moment–curvature state and φ_j and M_j are the current state. E and I represent the elastic modulus and the moment of inertia of the uncracked section. The unloading factor ξ is between 0 and 1; $\xi =$ 0 and 1 indicates no curvature recovery and unloading elastically with initial stiffness EI, respectively. In the present study, an unloading factor ξ is assumed to be 1 as the cracks in the unloading zone close due to high fibre content. For a section in the localized zone, the unloading curvature is determined from the descending portion of the moment–curvature diagram (M_{max} to M_{fail}). Once the curvature along the length of the beam is determined, the mid-span deflection can be obtained by the moment area method.

4. Accelerated aging of GFRC

The aging effects on mechanical responses of GFRC previously studied by Marikunte *et al.*[10] were analyzed with the proposed model. Only two test series of the control and metakaolin mixes were considered. Both contain the same amount of alkali-resistant (AR)-glassfibre content of 5% by weight of composite and the mix proportions are given in Table 2. The size of specimens was approximately 50.8 × 10.2 × 228 mm with a clear span of 203 mm. Each mix series was subjected to three levels of aging: unaged (moisture cured for 28 days), 28 and 84 days of accelerated aging simulated by submerging specimens in hot water. Four-point bending tests were conducted to evaluate its flexural performance.

Mix ingredients	**Mixes**	
	Control (kg)	**Metakaolin (kg)**
Cement	100	100
Sand	100	100
Metakaolin	–	25
Water	27.2	44
Polymer	9.8	12.3
Superplasticiser	1.8	3.0
Glassfibres	5% by weight of composite	5% by weight of composite

Table 2: Details of test series and mix proportions

4.1. Inverse analysis

Since the compressive strength of concrete materials is several times higher than their tensile strength, tensile characteristics control the flexural behaviour of a beam specimen. The tensile properties of GFRC can therefore be estimated by inverse analysis from flexural response. For typical high-dosage-fibre GFRC that shows deflection hardening followed by brittle failure in the post-peak region, it is sufficient to describe the material behaviour with four parameters: Young's modulus E, first cracking strain ε_{cr}, post-cracking modulus E_{cr} and strain at peak stress ε_{trn} (or transition strain). The constant stress in the last post-crack region σ_{cst} for all test series was assumed to be zero as the experimental post-peak responses appear very brittle. The compressive response was assumed to be in the linear elastic range as compressive strength is relatively high compared to weaker tensile strength.

Prior to conducting inverse analysis, load–deflection responses of four samples were first averaged to obtain a representative curve and then converted to the equivalent flexural stress by:

$$\sigma_{equiv} = \frac{PL}{bh^2} \qquad (9)$$

The inverse analysis was performed by first adjusting Young's modulus until the initial slopes of the predicted and experimental flexural stress–deflection responses were fitted. Next, the first cracking strain and post-cracking tensile modulus E_{cr} were adjusted until the predicted post-crack response matched the limit of proportionality (LOP) of the experiments. Finally, the strain at peak stress ε_{trn} (or transition strain) was adjusted until the predicted and experimental peak stresses were coincident.

Figure 4 shows the inverse analysis results of the two mixes at three aging levels. Fig. 4(a) shows the predicted and experimental flexural stress deflection of the control mixes. The initial slope of the unaged response becomes stiffer when it ages to 28 days and then softens until the specimen is aged 84 days. The peak strength of the specimen decreases continuously from unaged to 84 days of aging. Fig. 4(b) reveals the obtained tension model from the inverse analysis, showing that the shape of the tension model follows the shape of equivalent flexural stress but the magnitudes are lower by as much as 50%. This difference is due to the stress definitions assumed by each model. The equivalent flexural stress assumes a linear elastic stress distribution, having a triangular shape, for pre- to post-crack responses, while the proposed model assumes a more realistic tensile stress shape as previously described in Fig. 1(b).

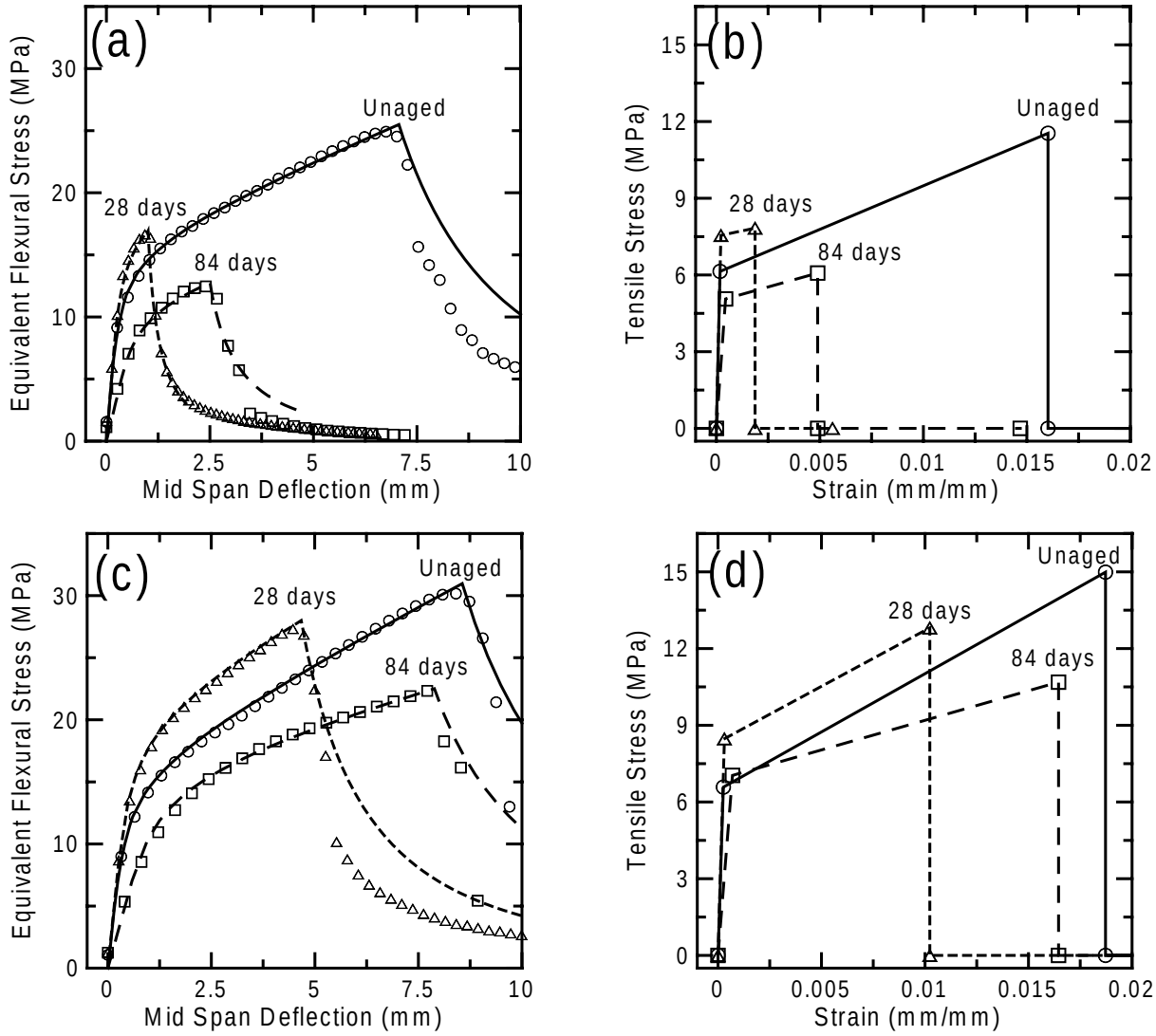

Figure 4: The results from inverse analysis of flexural test data: (a) and (c) equivalent flexural stress deflection responses of control and metakaolin mixes; (b) and (d) the obtained tension models for control and metakaolin mixes

When using metakolin in the mix, the long- term flexural behaviour shows the improvement compared to the control mix as can be seen in Fig. 4(a) and (c). Similar to the control mix, the initial slope of flexural response slightly increases between unaged and 28 days of aging and then decreases when it reaches 84 days. The flexural strength continuously drops from unaged to 84 days but is much less severe than the drop in the control mix. The ductility, as defined by an area under the curve, decreases slightly with aging and this reduction is less severe than in the control mix. Fig 4(d) reveals the inverse analysis results, which resemble the equivalent flexural stress but less than half the magnitude.

With three data points for aging levels, the relationship between material parameters and aging levels can be established using a quadratic function as shown in Fig. 5. Only the relationship for strain at maximum stress of the control mix in Fig. 5(d) needs to be approximated by a linear function as the quadratic form will result in a negative strain between ages 28 and 56 days, which is impossible. The relationships between four sensitive parameters and age t in equivalent accelerated aging days for the control mix is established as follows:

$$E(t) = 3.411\times10^{4} + 1.471\times10^{2}t - 4.973t^{2} \quad (10)$$

$$\varepsilon_{cr}(t) = 1.80\times10^{-4} + 5.655\times10^{-7}t + 3.082\times10^{-8}t^{2} \quad (11)$$

$$E_{cr}(t) = 3.411\times10^{2} - 8.401t + 8.392\times10^{-2}t^{2} \quad (12)$$

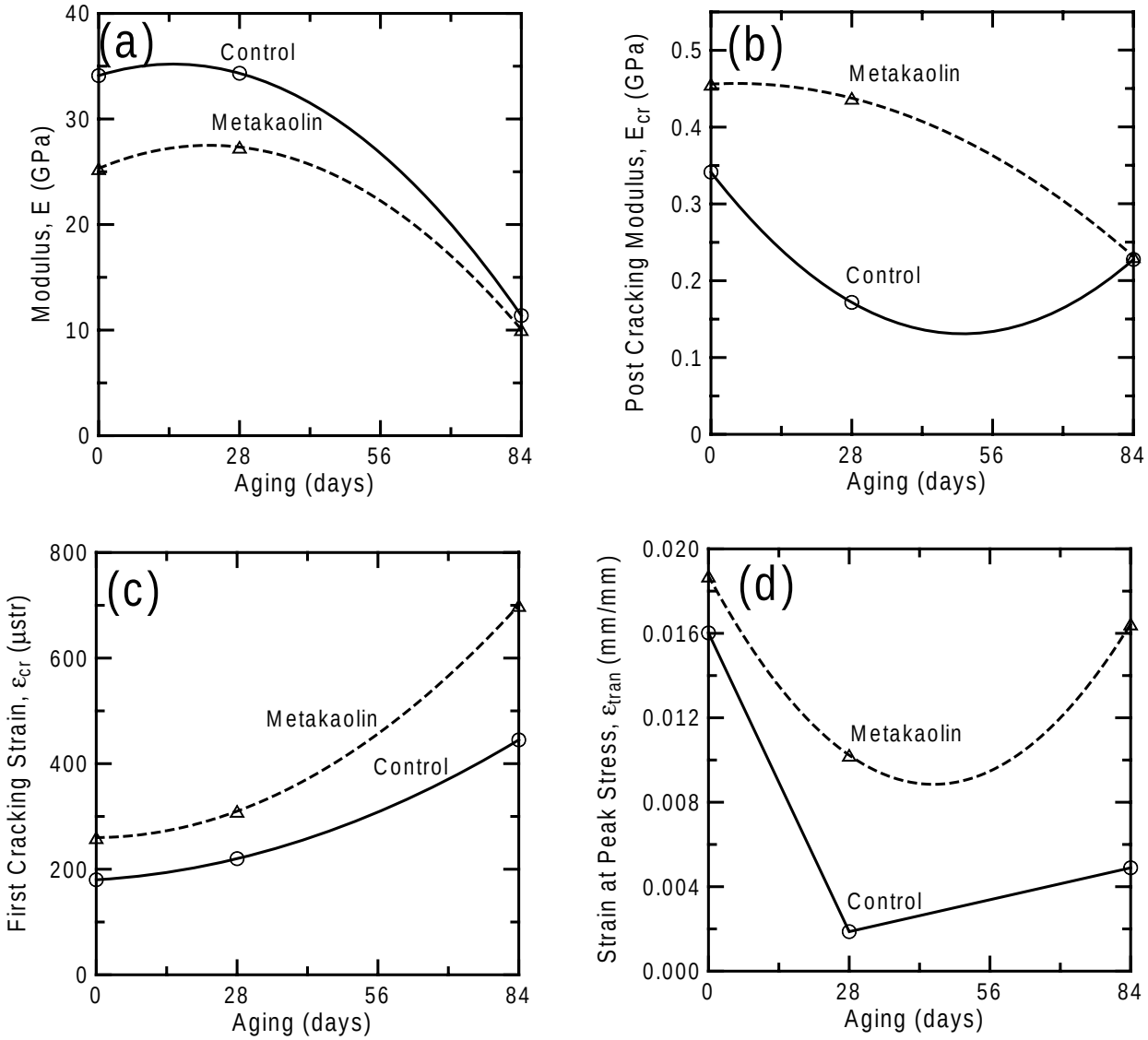

Figure 5: Material time-dependent parameters: (a) Young's modulus; (b) post-cracking modulus; (c) first cracking tensile strain; (d) strain at peak stress

$$\varepsilon_{trn}(t) = \begin{cases} 0.1602x10^{-1} - 0.5055x10^{-3}\ t & for\ \ 0 \le t \le 28 \\ 0.3575x10^{-3} + 0.5402x10^{-4}\ t & for\ \ 28 \le t \le 84 \end{cases} \quad (13)$$

Another set of relationships for metakaolin mix can be expressed as follows:

$$E(t) = 2.531\times10^{4} + 1.994\times10^{2}t - 4.535t^{2} \quad (14)$$

$$\varepsilon_{cr}(t) = 2.60\times10^{-4} + 5.952\times10^{-8}t + 6.165\times10^{-8}t^{2} \quad (15)$$

$$E_{cr}(t) = 4.556\times10^{2} + 3.603\times10^{-1}t + 3.607\times10^{-2}t^{2} \quad (16)$$

$$\varepsilon_{trn}(t) = 1.872\times10^{-2} + 4.413\times10^{-4}t + 4.932\times10^{-6}t^{2} \quad (17)$$

Mixes	Age	b	d	E	E_{cr}	ε_{cr}	ε_{trn}	η	α
	(days)	(mm)	(mm)	(GPa)	(GPa)	(μ_{str})			
Control	0	50.1	10.2	34.11	0.3411	180	0.01602	0.010	89.0
	28	49.7	10.4	34.33	0.1716	220	0.00187	0.005	8.5
	84	50.2	10.7	11.38	0.2275	445	0.00490	0.020	11.0
Metakaolin	0	50.1	10.5	25.31	0.4556	260	0.01872	0.018	72.0
	28	49.9	10.5	27.34	0.4374	310	0.01023	0.016	33.0
	84	50.0	10.6	10.06	0.2314	700	0.01645	0.023	23.5

Table 3: Obtained material parameters for the model from inverse analysis

4.2. Simulations of aging in GFRC

Once the relationships between material parameters and accelerated aging were established, the changes of moment–curvature response with time can be simulated. At any age between 0 to 84 days, the four material parameters required for the model can be calculated from equations (10)–(13) for the control mix and equations (14)–(17) for the metakaolin mix. The moment–curvature response can be generated by equations (6) and (7) and the expressions given in Table 1. Fig. 6 compares the long-term flexural behaviour as material properties age with time. It can be noted that the shape of the moment–curvature responses resemble the shapes of equivalent flexural stress deflection previously presented in Fig. 4(a) and (c). Fig. 6(a) reveals that the moment capacity of the control mix decreases continuously with time while the ductility rapidly decreases and then slightly increases. On the other hand, the response of the metakaolin specimen is only a slight drop in strength and ductility. The performance of the metakaolin is better than the control mix at all times. This procedure can also be applied to other alternative admixtures that are being considered for increasing the long-term durability of GFRC composites. The results from simulations can be used in practice by correlating one day of accelerated aging in hot water at 50°C with one day of natural aging under different mean temperatures; for example, one day of accelerated aging equals 18 days in Miami, USA which has a mean natural temperature of 24°C or 160 days in Montreal Canada that has a mean temperature of 7°C[3].

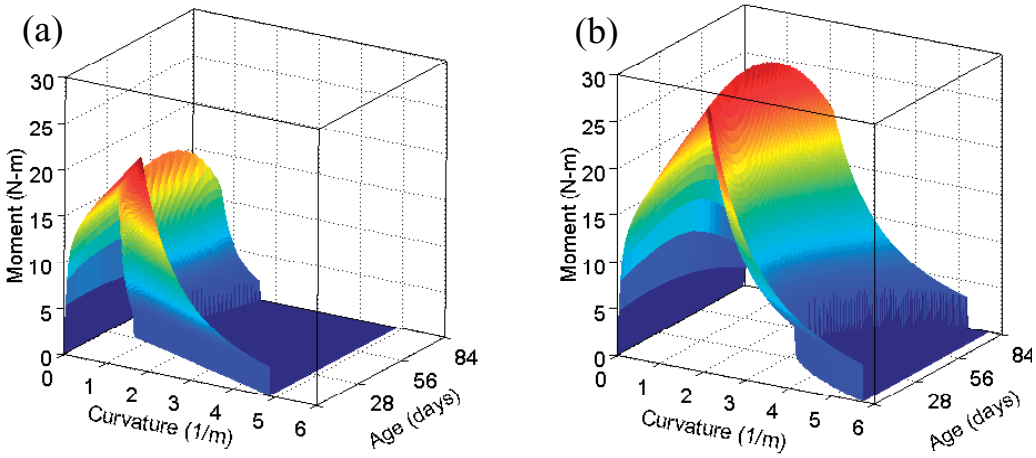

Figure 6: Simulation of long-term flexural behavior for GFRC: (a) control mix; and (b) metakaolin mix

5. Conclusions

A model was proposed to use flexural load–deflection data in order to characterize and simulate the aging effect in GFRC mixtures. The tensile material properties were obtained by inverse analysis of the flexural responses. This allows the material properties to be determined from flexural quality control tests and applied in various analysis and design packages such as the finite-element method. Material responses are described by four parameters: Young's modulus, first cracking tensile strain, post-cracking modulus and strain at peak stress. With calibrated material parameters at three accelerated aging levels, quadratic and linear functions were employed to establish the material-dependent properties and used to simulate the changes in moment–curvature response as it degrades with time. The simulation results clearly show the effect of using metakaolin in preventing deterioration of the GFRC. The moment and ductility of the metakaolin specimen slightly decrease compared to those of the control mix. In this study, the range of the model is restricted to one dosage of AR-glassfibre at 5% by weight but it can be improved if more test data on different levels of fibre, matakaolin and ages are available.

6. Acknowledgement

The authors gratefully acknowledge the support of the National Science Foundation, Award No. 0324669-03; and Programme manager Dr P. Balaguru for his support of this research.

References

1. Mobasher, B. and Shah, S.P. Test parameters for evaluating toughness of glass-fiber reinforced concrete panels. ACI Materials Journal, Vol. 86, No. 5, Sept.–Oct. 1989, pp. 448–458.

2. Soroushian, P., Tlili, A., Yohena, M. and Tilsen, B.L. Durability characteristics of polymer-modified glass fiber reinforced concrete. ACI Materiasl Journal, Vol. 90, No. 1, Jan.–Feb. 1993, pp. 40–49.

3. Litherland, K.L., Oakley, D.R. and Proctor, B.A. The use of accelerated aging procedures to predict the long term strength of GRC composites. Cement and Concrete Research, Vol. 11, No. 3, May 1981, pp. 455–466.

4. Proctor, B.A. Past development and future prospect for GRC materials. Proceedings of an International Congress on Glass Fibre Reinforced Cement, Paris, Nov. 1981. The Glass Fibre Reinforced Cement Association, Gerrards Cross, pp. 50–67.

5. Soranakom, C. and Mobasher, B. Correlation of tensile and flexural responses of strain softening and strain hardening cement composites. Cement and Concrete Composites (in press Jan. 2008).

6. Soranakom, C. and Mobasher, B. Flexural modeling of strain softening and strain hardening fiber reinforced concrete. Proceedings of the Fifth International RILEM Workshop, High Performance Fiber Reinforced Cement Composites (HPFRCC5), Mainz, Germany, July 2007, pp. 155–164.

7. Naaman, A.E. and Reinhardt, H.W. Proposed classification of HPFRC composites based on their tensile response. Materials and Structures, Vol. 39, June 2006, pp. 547–555.

8. Ulfkjaer, J.P., Krenk, S. and Brincker, R. Analytical model for fictitious crack propagation in concrete beams. Journal of Engineering Mechanics, Vol. 121, No. 1, Jan. 1995, pp. 7–15.

9. Olesen, J.F. Fictitious crack propagation in fiber-reinforced concrete beams. Journal of Engineering Mechanics, Vol. 127, No. 3, March 2001, pp. 272–280.

10. Marikunte, S., Aldea, C. and Shah, S.P. Durability of glass fiber reinforced cement composites: effect of silica fume and metakaolin. Advanced Cement Based Materials, Vol. 5, No. 3–4, Apr.–May 1997, pp. 100–108.